J IRAN CHEM SOC
DOI 10.1007/s13738-016-0807-0

ORIGINAL PAPER

Effect of the substitutional groups on the electrochemistry, kinetic of thermal decomposition and kinetic of substitution of some uranyl Schiff base complexes

Zahra Asadi[1] · Rahele Nasrollahi[1] · Michal Dusek[2] · Karla Fejfarova[2] · Mohammad Ranjkeshshorkaei[1] · Fahimeh Dehghani Firuzabadi[1]

Received: 5 October 2015 / Accepted: 4 January 2016

Abstract Uranyl(VI) complexes, [UO_2(X-saloph)(solvent)], where *saloph* denotes *N*,*N*'-bis(salicylidene)-1,2-phenylenediamine and X = NO_2, Cl, Me, H; were synthesized and characterized by ^{1}H NMR, IR, UV–Vis spectroscopy, thermal gravimetry (TG), cyclic voltammetry, elemental analysis (C.H.N) and X-ray crystallography. X-ray crystallography of [UO_2(4-nitro-saloph)(DMF)] revealed coordination of the uranyl by the tetradentate Schiff base ligand and one solvent molecule, resulting in seven-coordinated uranium. The complex of [UO_2(4-nitro-saloph)(DMF)] was also synthesized in nano form. Transmission electron microscopy image showed nano-particles with sizes between 30 and 35 nm. The TG method and analysis of Coats-Redfern plots revealed that the kinetics of thermal decomposition of the complexes is of the first-order in all stages. The kinetics and mechanism of the exchange reaction of the coordinated solvent with tributylphosphine was investigated by spectrophotometric method. The second-order rate constants at four temperatures and the activation parameters showed an associative mechanism for all corresponding complexes with the following trend: 4-Nitro > 4-Cl > H > 4-Me. It was concluded that the steric and electronic properties of the complexes were important for the reaction rate. For analysis of anticancer properties of uranyl Schiff base complexes, cell culture and MTT assay was carried out. These results showed a reduction of jurkat cell line concentration across the complexes.

✉ Zahra Asadi
zasadi@shirazu.ac.ir

[1] Chemistry Department, College of Sciences, Shiraz University, Shiraz 71454, Islamic Republic of Iran

[2] Institute of Physics ASCR, v.v.i, Na Slovance 2, 821182 Prague, Czech Republic

Keywords Nano uranyl schiff base complex · Kinetic study · X-ray crystallography · Anticancer activity · TG · Cyclic voltammetry

Introduction

Schiff base ligands form stable complexes with most transition metal ions, which can be used as biological model compounds [1–5]. Coordination complexes with substituted salicylaldehydes have structures with diverse stereochemistry and a wide range of bonding interactions [6–9].

The linear dioxoactinoid (VI) ions, e.g., UO_2^{2+}, have all their exchangeable ligands in the plane perpendicular to the linear axis. The "-yl" oxygens are substitution inert [10] except in the case when the ion is excited by UV light [11–13]. This coordination geometry indicates that the pathway for ligand substitution reactions should be located in, or close to, this plane, a very different situation from those encountered in most other coordination geometries. However, studies of the mechanisms for ligand substitutions in uranium (VI) complexes are scarce. Substitution mechanisms have been discussed in [14, 15] and the experimental evidence seems to favor dissociative (D) or dissociative interchange (I_d) mechanisms.

In this paper some tetradentate Schiff base ligands and their uranyl complexes were synthesized and characterized by ^{1}H NMR, IR, UV–vis spectroscopy, thermal gravimetry (TG), cyclic voltammetry (CV), elemental analysis (C.H.N), and X-ray crystallography. Because of the importance of nano-structures in basic science as well as for technological applications [16–18], we also prepared one of the complexes in nano form. X-ray crystallography and TG revealed that one solvent molecule was coordinated weakly to the uranium center, in comparison with the Schiff base

Published online: 18 January 2016

and *trans* oxides. Thus it was interesting to study the kinetics of exchange of this solvent molecule with tributylphosphine and the parameters affecting the rate constants such as the electronic and the steric ones. From this point of view the effect of substitutional groups on the redox potential of these complexes was studied. The thermal stability and the kinetics of thermal decomposition of these complexes was also studied and revealed that only one solvent molecule is coordinated to the central uranium. Beside them anticancer activity of these complexes was also studied.

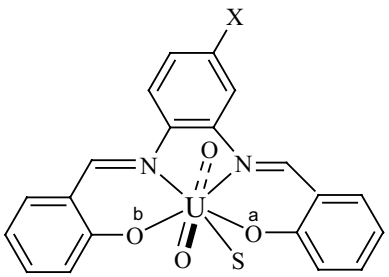

Fig. 1 Structural representation of the uranyl(VI) Schiff base complex X = H, Me, NO_2, Cl, and S = solvent

Experimental

Chemicals and apparatus

1,2-phenylenediamine, 4-chloro-1,2-phenylenediamine, 4-methyl-1,2-phenylenediamine, 4-nitro-1,2-phenylenediamine, salicylaldehyde, tri-*n*-butylphosphine (PBu_3), methanol (MeOH), acetonitrile (CH_3CN), potassium bromide (KBr), uranylacetatedihydrate $UO_2(OAc)_2$, DMSO-d_6, $CDCl_3$, tetrabutylammuniumperchlorate (Bu_4NClO_4), and diethyl ether were purchased commercially.

All of the scanning UV–vis spectra were recorded by using Perkin-Elmer Lambda 2 spectrophotometer equipped with a Lauda-ecoline-RE 104 thermostat. FT-IR spectra were run on a Shimadzu FTIR-8300 spectrophotometer. ^{1}H NMR spectra were recorded on a Bruker Avance DPX-250 spectrometer in $CDCl_3$ or DMSO-d_6 solvents at 250 MHz. Elemental analysis (C.H.N) was performed on a C.H.N Thermo Finnigan Flash EA1112 analyzer. Cyclic voltammetry (CV) spectra were obtained by using Auto lab 302 N, a three-electrode system was utilized, i.e., a glassy carbon working electrode, a reference electrode (Ag/Ag^+ in TBAP/acetonitrile solution), and a Pt auxiliary electrode. Tetrabutylammonium perchlorate (TBAP) was used as supporting electrolyte. Melting point was measured by BUCHI 535. Thermal gravimetric (TG) analyses were recorded on Perkin-Elmer Pyris Diamond model. Transmission electron microscopy (TEM) was performed on a Zeiss EM10C Acc voltage 60 kV set. Incubator and ELISA reader (Bio-Tek's ELx808, USA) were used for anticancer studies. X-ray crystallography was performed by the four-cycle diffractometer Gemini of Agilent Technologies (2012).

Synthesis of the ligands

All the tetradentate Schiff base ligands were synthesized by the reaction of salicylaldehyde and different diamines with the ratio of (2:1) in methanol solvent under reflux for 2–4 h. After cooling and evaporating the solvent, products were filtered and washed with diethyl ether (Fig. 1).

N,*N*'-bis(salicylidene)-1,2-phenylenediamine (*saloph*): Yield: 72 %, Color: orange, m.p. = 150 °C, Anal. Found (Calc.): $C_{20}H_{16}N_2O_2$ (316.36): C, 75.86(75.93); H, 5.04(5.10); N, 8.65(8.85). IR (KBr, cm^{-1}): 3485(υ_{O-H}), 2900–3031(υ_{C-H}), 1611($\upsilon_{C=N}$), 1481($\upsilon_{C=C}$), ^{1}H NMR (250 MHz, $CDCl_3$, room temperature): δ(ppm) = 6.88–7.38 (m, 12H, ArH), 8.61(s, 2H, HC=N), 12.90 (s, 2H, OH). Uv–vis. (acetonitrile): λ_{max} (nm), ε (M^{-1} cm^{-1}) = 206(sh), 226(sh), 265(~82,352), 328(~41,746).

N,*N*'-bis(salicylidene)-4-Methyl-1,2-phenylenediamine (*4-Mesaloph*): Yield: 95 %, Color: yellow, m.p. = 111 °C, Anal. Found (Calc.): $C_{21}H_{18}N_2O_2$(330.38): C, 75.98(76.34); H, 5.43(5.49); N, 8.55(8.48). IR (KBr, cm^{-1}): 3463(υ_{O-H}), 2900–3010(υ_{C-H}), 1612($\upsilon_{C=N}$), 1488($\upsilon_{C=C}$), ^{1}H NMR (250 MHz, DMSO-d_6, room temperature): δ(ppm) = 2.36 (s, 3H, CH_3), 6.91–7.66 (m, 11H, ArH), 8.90(s, 2H, HC=N), 12.95 (s, H, OH^a), 13.09 (s, H, OH^b). UV–vis. (acetonitrile): λ_{max} (nm), ε (M^{-1} cm^{-1}) = 263(~21,333), 326(~17,833).

N,*N*'-bis(salicylidene)-4-chloro-1,2-phenylenediamine (4-Clsaloph): Yield: 81 %, Color: yellow, m.p. = 138.5 °C, Anal. Found (Calc.): $C_{20}H_{15}N_2O_2Cl$ (350.80): C, 68.39(68.48); H, 4.83(4.31); N, 7.90(7.99). IR (KBr, cm^{-1}): 3417(υ_{O-H}), 2900–3150(υ_{C-H}), 1620($\upsilon_{C=N}$), 1481($\upsilon_{C=C}$), ^{1}H NMR (250 MHz, DMSO-d_6, room temperature, TMS): δ(ppm) = 6.60–7.66 (m, 11H, ArH), 8.8 (s, 1H, H^bC=N), 8.9 (s, 1H, H^aC=N), 12.5 (s, 1H, OH^b), 12.7 (s, 1H, OH^a). UV–vis. (acetonitrile): λ_{max} (nm), ε (M^{-1} cm^{-1}) = 213(~55,357), 255(sh), 327(~18,452).

N,*N*'-bis(salicylidene)-4-nitro-1,2-phenylenediamine(4-Nitrosaloph): Yield: 72 %, Color: yellow, m.p. = 201 °C, Anal. Found (Calc.):$C_{20}H_{15}N_3O_4$(361.36): C, 66.51(66.48); H, 4.14(4.18); N, 11.69(11.63). IR (KBr, cm^{-1}): 3425(υ_{O-H}), 2900–3025(υ_{C-H}), 1612 ($\upsilon_{C=N}$), 1473($\upsilon_{C=C}$), ^{1}H NMR (250 MHz, $CDCl_3$, room temperature, TMS): δ(ppm) = 6.65–8.33 (m, 11H, ArH), 8.95 (s, 1H, H^bC=N), 9.0 (s, 1H, H^aC=N), 12.24 (s, 1H, OH^b), 12.57 (s, 1H, OH^a). UV–vis. (acetonitrile): λ_{max} (nm), ε (M^{-1} cm^{-1}) = 276(~28,035), 342(sh).

Synthesis of uranyl complexes

Uranyl complexes were prepared by addition of uranyl acetate dihydrate (5 mmol, 20 ml methanol), into a hot methanolic solution of the Schiff base (5 mmol, 10 ml) (1:1 molar ratio). The color of the solution changed to orange-red in a few minutes. The mixture was then refluxed for 3 h. The precipitate was washed with ether, followed by drying at 50 °C in vacuum.

Synthesis of a nano uranyl Schiff base complex

Nano uranyl Schiff base complex was synthesized by addition of methanolic solution of uranyl acetate dihydrate (5 mmol in 50 ml methanol) to the hot methanolic solution of Schiff base (5 mmol in 60 ml methanol). Metal solution was added dropwisely in about 6–7 h. The mixture was then refluxed for 24 h. Transmission electron microscopy (TEM) showed nano-particles with sizes between 30 and 35 nm (Fig. 2).

$[UO_2$(saloph)(MeOH)] yield: 79 %, color: orange, m.p. > 250 °C, anal. found (Calc.): $C_{21}H_{18}N_2O_5U$ (616.41): C, 40.88(40.92); H, 2.92(2.94); N, 4.57(4.54). IR (KBr, cm^{-1}): 3456(υ_{O-H}), 2885–3038(υ_{C-H}), 1607($\upsilon_{C=N}$), 1445($\upsilon_{C=C}$), 908($\upsilon_{U=O}$), 540(υ_{U-N}), 440(υ_{U-O}). ^{1}H NMR (250 MHz, DMSO-d_6, room temperature): δ(ppm) = 3.14 (d, 3H, MeOH), 4.07 (q, 1H, MeOH), 7.50–7.80 (m, 8H, ArH), 9.59 (s, 2H, HC = N). UV–vis. (acetonitrile): λ_{max} (nm), ε (M^{-1} cm^{-1}) = 240(~9769), 278(sh), 341(4611), 413(sh).

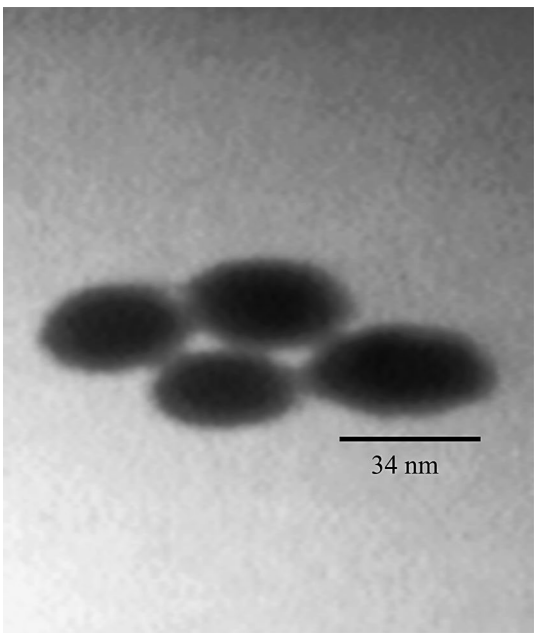

Fig. 2 TEM image of $[UO_2$(4-NO_2-saloph)(MeOH)] nano-particles

$[UO_2$(4-Me-saloph)(MeOH)] yield: 87 %, color: light red, m.p. > 250 °C, anal. found (Calc.): $C_{22}H_{20}N_2O_5U$ (630.44): C, 42.03(41.91); H, 3.18(3.20); N, 4.54(4.44). IR (KBr, cm^{-1}): 3450(υ_{O-H}), 2950–3050(υ_{C-H}), 1600($\upsilon_{C=N}$), 1440($\upsilon_{C=C}$), 906($\upsilon_{U=O}$), 557(υ_{U-N}), 447(υ_{U-O}). ^{1}H NMR (250 MHz, DMSO-d_6, room temperature): δ(ppm) = 2.48 (s, 3H, CH_3), 3.14 (d, 3H, MeOH), 4.09 (q, 1H, MeOH), 6.67–7.80 (m, 11H, ArH), 9.48 (s, 1H, H^aC=N), 9.67 (s, 1H, H^bC=N). UV–vis. (acetonitrile): λ_{max} (nm), ε (M^{-1} cm^{-1}) = 243(~41,041), 278(sh), 346(~19,375), 414(sh).

$[UO_2$(4-Cl-saloph)(MeOH)] yield: 75 %, color: dark red, m.p. > 250 °C, anal. found (Calc.): $C_{21}H_{17}N_2ClO_5U$ (650.86): C, 38.97(38.75); H, 2.53(2.63); N, 4.20(4.30). IR (KBr, cm^{-1}): 3350(υ_{O-H}), 2927–3068(υ_{C-H}), 1600($\upsilon_{C=N}$), 1438($\upsilon_{C=C}$), 902($\upsilon_{U=O}$), 580(υ_{U-N}), 439(υ_{U-O}). ^{1}H NMR (250 MHz, DMSO-d_6, room temperature): δ(ppm) = 3.15 (d, 3H, MeOH), 4.11 (q, 1H, MeOH), 6.67–7.93 (m, 11H, ArH), 9.58 (s, 1H, H^bC=N), 9.67 (s, 1H, H^aC=N). UV–vis. (acetonitrile): λ_{max} (nm), ε (M^{-1} cm^{-1}) = 244.4(~44,231), 284(~28,125), 342(~18,269), 415(sh).

$[UO_2$(4-nitro-saloph)(MeOH)] yield: 87 %, color: red, m.p. > 250 °C, anal. found (Calc.): $C_{21}H_{17}N_3O_7U$ (661.41): C, 38.31(38.14); H, 2.54(2.59); N, 6.40(6.35). IR (KBr, cm^{-1}): 3350(υ_{O-H}), 2927–3067(υ_{C-H}), 1604($\upsilon_{C=N}$), 1438($\upsilon_{C=C}$), 902.6($\upsilon_{U=O}$), 551(υ_{U-N}), 439.7(υ_{U-O}). ^{1}H NMR (250 MHz, DMSO-d_6, room temperature): δ(ppm) = 3.16 (d, 3H, MeOH), 4.08 (q, 1H, MeOH), 6.70–8.66 (m, 11H, ArH), 9.63 (s, 1H, H^bC=N), 9.74 (s, 1H, H^aC=N). UV–vis. (acetonitrile): λ_{max} (nm), ε (M^{-1} cm^{-1}) = 304(~20,416), 341(sh), 422(~11,041).

Crystal growth for X-ray crystallography

Slow diffusion of diethyl ether into a solution of the metal complex in dimethylformamide (DMF) at room temperature produced crystals of the uranyl complex $[UO_2$(4-NO_2-saloph)(DMF)]. The crystals were intensely colored. The preparation from DMF/Et_2O gave better single crystals compared with the preparation from acetonitrile, which was also attempted. The data were collected on Gemini diffractometer with Atlas CCD detector using graphite monochromated Mo-Kα radiation (λ = 0.7107 Å) and corrected for absorption using the CrysAlisPro software. The structure was solved by the charge flipping method by program Superflip [19] and refined by full matrix least squares on F^2 with JANA 2006 program [20].

Cell culture and MTT assay for analysis of anticancer properties of complexes

The cancer cell lines were cultured in RPMI 1640 Medium (HiMedia, Mumbai, India) supplemented with 10 % Fetal

Calf Serum (FCS) (Biochrom, Germany). 100 IU/ml of penicillin and 100 mg/ml of streptomycin were also added to the media as antibiotics to control the growth of contaminating microorganisms. The cells were cultured in 96 well tissue culture plates (Greiner, USA), and kept at 37 °C in a humidified atmosphere of 5 % CO_2 in a CO_2 incubator. All the experiments were done using cancer cell line (Jurkat) of 10–15 passage. The growth inhibitory effect of uranyl complexes (D, E, F) toward the cancer cells was measured using 3-(4,5-dimethylthiazol-2-yl)-2,5-diphenyltetrazoliumbromide (MTT) assay. *D*, *E* and *F* are: $D = [UO_2$(4-Cl-saloph)(DMSO)], $E = [UO_2$(saloph)(DMSO)] and $F = [UO_2$(4-Me-saloph)(DMSO)].

The cleavage and conversion of the soluble yellowish MTT to the insoluble purple formazan by active mitochondrial dehydrogenises of living cells has been used to develop an assay system alternative to other assays for measurement of cell proliferation [21]. The drug treatment performed as the harvested cells were seeded into 96-well plate (2.5×10^4 cell/well) with varying concentrations of the sterilized uranyl complexes (0–100 μM) and incubated for 24 and 48 h. Four hours to the end of incubations, 25 μl of MTT solution (5 mg/ml in PBS) was added to each well containing fresh and cultured medium. Finally, the insoluble formazan was dissolved in solution containing 10 % SDS and 50 % DMF (left for 1 h at 37 °C in dark conditions) and optical density (OD) was read against reagent blank with multi well scanning spectrophotometer (ELISA reader, Bio-Tek's ELx808, USA) at a wavelength of 570 nm. The absorbance is a function of concentration of converted dye. The OD value of study groups was divided by the OD value of untreated control and presented as percentage of control (as 100 %). Also the values of IC_{50} (the concentrations required for 50 % growth inhibition), after 24 h of incubation with the complexes were calculated.

Kinetic studies of the exchange reactions

A solution of the uranyl complexes with known concentration ($2.5–5) \times 10^{-5}$ M in acetonitrile was prepared. 2.5 ml of each complex was poured in a cell, and a known excess concentration of PBu_3 solution in acetonitrile (runs from 10.0 to 40.0 ± 0.1 °C) was added to the complex by using a microsyringe. After rapid stirring by a microsyringe, the absorbance in the UV–vis region was monitored with time. The kinetics was followed at a wavelength of maximum absorbance, where the difference in the absorbance between the substrate and the product was the largest (λ_{max}). This wavelength was different for each complex.

Synthesis of the kinetic product

To a refluxing solution of $[UO_2$(saloph)(solvent)] (0.017 mmol), in acetonitrile (25 ml) tri-*n*-butylphosphine (0.017 mmol) was added. The reaction mixture was refluxed for 24 h under nitrogen atmosphere. The resulting oil was grinded with *n*-hexane to extract impurities, and finally a powdery product was obtained.

$[UO_2$(saloph)$(PBu_3)]$: yield: 87 %, color: orange, m.p. = 150–155 °C, anal. found (calc.): $C_{32}H_{41}N_2O_4U$ (755.72): C, 50.71(50.86); H, 5.54(5.47); N, 3.60(3.71). ^{1}H NMR (250 MHz, DMSO-d_6, room temperature): δ(ppm) = 0.82 (t, 9H, CH_3), 1.33 (m, 12H, CH_2), 1.61 (t, 6H, CH_2), 6.80–7.68 (m, 12H, ArH), 9.34 (s, 2H, HC=N). IR (KBr, cm^{-1}): 2869–3056 (υ_{C-H}), 1604($\upsilon_{C=N}$), 1535($\upsilon_{C=C}$), 1188 (υ_{C-O}), 895($\upsilon_{U=O}$), 540(υ_{U-N}), 439(υ_{U-O}).

Results and discussion

Characterization of the complexes

Crystal structure determination of $[UO_2$(4-NO_2-saloph)(DMF)] complex

Crystal data, data collection, and structure refinement details are listed in Table 1. The ORTEP view of this complex is shown in Fig. 3, with selected bond parameters

Table 1 Crystal data, data collection and structure refinement details for $[UO_2$(4-NO_2-saloph)(DMF)]

	Complex
Formula	$C_{23}H_{20}N_4O_7U$
Formula weight	702.46
Crystal system	Monoclinic
Space group	$P2_1/c$
a (Å)	33.0314 (7)
b (Å)	7.76870 (10)
c (Å)	27.7752 (6)
α (°)	90
β (°)	105.444(2)
γ (°)	90
vol/Å^3	6870.06
Z,*Z*′	12.3
$D_{calcd.}$ (Mg m^{-3})	2.0375
Abs. coeff. (mm^{-1})	7.141
F(000)	4008.0
*R*1, *wR*2 [$I > 3\sigma(I)$]	0.0326, 0.0581
*R*1, *wR*2 (all data)	0.0550, 0.0337

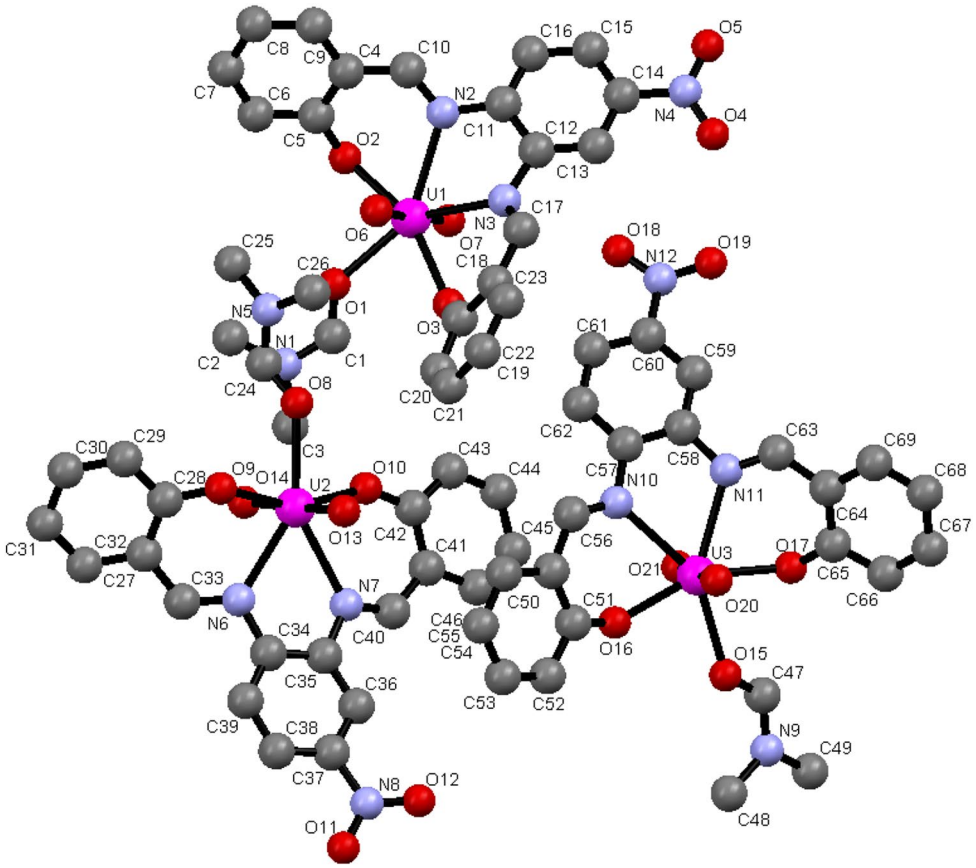

Fig. 3 Molecular structure of $[UO_2(4\text{-}NO_2\text{-saloph})(DMF)]$, (50 % probability ellipsoids, H atoms omitted for clarity)

listed in Table 2. The complex contained three symmetry-independent molecules, which are chemically identical but they differ considerably by, e.g. angles between the aromatic rings. The molecules are compared in Table 2.

For each molecule, uranium had a pentagonal–bipyramidal coordination geometry with an axial O=U=O [22]. The ligand bound in a tetradentate fashion along the equatorial axis of the uranyl ion and a solvent molecule occupied the fifth coordination site in the equatorial plane. The geometry around each uranium center deviates from the planar geometry as can be recognized from the angles in Table 2.

One DMF molecule was coordinated to each of the three symmetry-independent molecules. The bond length between U and O (oxygen of DMF) was longer than U with O (Schiff base oxygens), suggested that the coordination of DMF was not as strong as the coordination of the Schiff base [23]. The angle between oxygen atoms of axial oxygens (UO_2) was 175.9°, 177.7° and 177.3° that were not equal and were less than 180°.

Notable feature was the anharmonic behavior of uranium, namely U1. For this atom, displacement described

Table 2 Selected bond distances (Å) and angles (°) for $[UO_2(4\text{-}NO_2\text{-saloph})(DMF)]$

U1–O1	2.426(4)	U2–O9	2.268(3)
U2–O8	2.421(3)	U2–O10	2.231(3)
U3–O15	2.431(3)	U3–O16	2.220(3)
U1–O6	1.776(3)	U3–O17	2.241(3)
U1–O7	1.779(3)	U1–N2	2.561(4)
U2–O13	1.775(3)	U1–N3	2.539(4)
U2–O14	1.785(3)	U2–N6	2.549(4)
U3–O20	1.784(3)	U2–N7	2.613(3)
U3–O21	1.786(3)	U3–N10	2.600(3)
U1–O2	2.225(3)	U3–N11	2.520(4)
U1–O3	2.283(3)	O2–U1–O3	157.1(1)
O2–U1–O7	175.9(2)	N2–U1–N3	62.6(1)
O13–U2–O14	177.7(1)	N2–C11–C16	123.0(4)
O20–U3–O21	177.3(1)	N3–C12–C13	124.2(4)
O16–U3–O17	154.9(8)	N7–C35–C36	123.5(4)
N10–U3–N11	63.5(1)	N6–C34–C39	121.4(4)
O9–U2–O10	157.2(1)	N11–C58–C59	122.2(4)
N6–U2–N7	63.9(1)	N10–C57–C62	123.8(4)

with an ellipsoid was not sufficient to explain strong residua in the difference Fourier map. On the other hand, description of U1 displacement with the third-order anharmonic tenzor explained sufficiently the residua and decreased significantly the *R*(obs) value (from 0.0326 to 0.0301). The deposited CIF does not contain this anharmonic model because it is not important for the crystal chemistry.

IR spectra

In the IR spectra of the ligand, bands observed in the regions 3402–3500 cm^{-1} were assigned to the OH group. The absence of these peaks in the complexes indicated the phenolic oxygen atoms coordinate to the metal center [24]. The bands at 2734–3055 cm^{-1} in the Schiff base ligands and complexes were related to aliphatic and aromatic C–H modes of vibrations. Data showed also a shift of the C=N vibration of the free ligand at 1597–1607 cm^{-1} region to a lower frequency in the complexes. This indicated the coordination of the azomethine nitrogen to uranium [25, 26]. The ring skeletal vibrations (C=C) were consistent in all derivatives in the region 1527–1572 cm^{-1} and unaffected by complexation.

The presence of the uranyl (VI) group can be easily proved by the strong IR band at 855–910 cm^{-1} due to the υ_3 O=U=O [27]. The bands at 472–662 cm^{-1} in the complexes were related to (υ_{U-N}) vibrations.

^{1}H NMR spectroscopy The ^{1}H NMR spectra of all the Schiff bases showed a singlet or doublet signal at 12.71–13.71 ppm corresponding to the hydrogen of the free OH group of salicylaldehyde. After coordination of Schiff base to the uranyl center, this signal was eliminated. The presence of a peak at 9.10–10.33 ppm, was due to the imine HC=N protons [28]. The azomethine proton signal shifted to lower fields which was also consistent with coordination of the metal to the nitrogen. The spectra exhibited a multiplet at 6.50–8.18 ppm for the aromatic hydrogens [29]. Aliphatic hydrogens showed signals at about 2–4 ppm.

In uranyl Schiff base complexes, MeOH was coordinated to metal center in the fifth coordination site in the equatorial plane of the uranyl Schiff base complexes. By using DMSO-d_6 as solvent for NMR studies, DMSO could expel methanol from coordination sphere. The presence of free MeOH in the solution caused that two signals were observed: methyl hydrogens had a doublet signal 3.14 ppm due to coupling with hydrogen of hydroxyl group and another peak was relevant to the hydrogen of OH group in 4.07 ppm as a quartet [30].

UV–Vis spectra

In ligands, the band in the region of 300–500 nm corresponded to the n–π^* transition of the lone pair electrons of nitrogen atom to the antibonding π^* orbital of –CH=N, and the band in the 200–300 nm region involved the π–π^* transition of the phenyl ring and the azomethine chromophore [31].

The peak around 330 and 350 nm of the complex could be assigned to the LMCT transition. In uranyl complexes, U(VI) has no electrons in valence shell; therefore U(VI) had only LMCT transitions. There were two kinds of charge transfer bands in the investigated uranyl complexes: one corresponding to the electron transfer from the axial oxygens to the central metal (2p of oxygen to 5f), and the other caused by the electron transfer from the phenolate group of the Schiff base ligand to the metal [32].

Thermal analysis

Thermal properties of the metal complexes were investigated up to 1000 ℃ under nitrogen atmosphere at a heating rate of 10 ℃/min. The TG spectra showed weight loss up to 100 ℃ indicating the presence of solvent (CH_3OH) molecule coordinated to metal. The absence of weight loss up to 80 ℃ indicated that there was no water molecule in the crystalline solid. All the complexes were decomposed in three steps. The first step of decomposition was related to the release of (MeOH) and the percent of found and calculated weight loss were nearly identical. Thermal decomposition data of uranyl complexes are collected in Table 3.

Kinetic aspects of thermal decomposition

DTG curves were used to study the kinetics of decomposition of the complexes. Coats-Redfern equation (1) was used to calculate kinetic parameters [33].

$$\log\left[\frac{-\log(1-a)}{T^2}\right] = \log\frac{A*R}{\beta E}\left[1-\frac{2RT}{E}\right] - \frac{E}{2.303RT} \quad (1)$$

In this equation; $a = \frac{(w_0-w_t)}{(w_0-w_f)}$. w_0 = initial mass of the sample; w_t = mass of the sample at temperature T; w_f = the final mass at a temperature when the mass loss is approximately unchanged; β = the heating rate; R = the gas constant. A plot of $\log\left[\frac{-\log(1-a)}{T^2}\right]$ against $1/T$ gives a straight line with the slope of $-E/2.303R$ (Fig. 4). A^* values can be calculated from the intercept of this plot. The entropy of activation $\Delta S^{\#}$. can be obtained using Eq. (2):

Table 3 Thermal decomposition data of uranyl complexes

Complex (F.W.)	TGA (Wt. loss %) calc. (found)	Temp. range in TG (°C)	Decomposition assignment
$[UO_2(saloph)(MeOH)]$ (616)	5.2(5.19)	140–400	Loss of MeOH
	12.8(12.33)	400–540	Loss of C_6H_4
	82(82.46)		Loss of $C_{14}H_{10}O_4N_2U$
$[UO_2(4\text{-Cl-saloph})(MeOH)]\cdot H_2O$ (668.8)	7.6(7.47)	40–340	Loss of MeOH + H_2O
	5.4(5.3)	340–425	Loss of Cl
	11.3(11.2)	420–625	Loss of C6H3
	75.7(75.94)		Loss of $C_{14}H_{10}O_4N_2U$
$[UO_2(4\text{-}NO_2\text{-saloph})(MeOH)]$ H_2O (679)	2.54(2.65)	30–185	Loss of H_2O
	4.36(4.7)	185–340	Loss of MeOH
	17.6(17.82)	340.695	Loss of $C_6H_3NO_2$
	75.5(75.26)		Loss of $C_{14}H_{10}O_4N_2U$
$[UO_2(4\text{-Me-saloph})(MeOH)]$ (630.4)	5.6(5.1)	100–220	Loss of MeOH
	14.4(14.27)	220–490	Loss of C7H6
	38(37.43)	490–1000	Loss of $C_{14}H_{10}N_2O_2$
	42.82(42.82)		Loss of UO_2

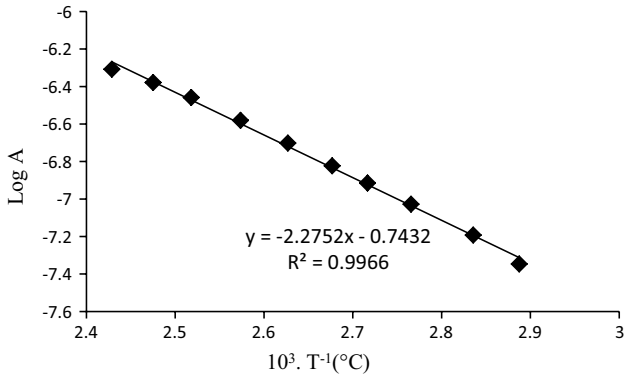

Fig. 4 Coats–redfern plots of $[UO_2(4\text{-Cl-saloph})(MeOH)]$ complex, $A = \log(W_f/W_f - W)$

$$A^* = \frac{KT_s}{h} e^{S^{\#}/T}. \tag{2}$$

where h = the Planck constant, K = the Boltzmann constant; T_s = the peak temperature obtained from DTG. The enthalpy and free energy of activation can be calculated using Eqs. (3, 4):

$$E = H^{\#} + RT \tag{3}$$

$$G^{\#} = H^{\#} - TS^{\#} \tag{4}$$

Activation parameters obtained for all the complexes are presented in Table 4. From these data it can be concluded that the Gibbs energy grew from stage to stage. This is probably due to the stable intermediate of the present stages. According to Coats-Redfern plots, in these complexes the kinetic of thermal decomposition is first-order in all stages [34].

The electrochemical study of uranyl complexes

Electrochemical studies of the uranyl *saloph* complexes were carried out in acetonitrile solution (1.00×10^{-3} M) and tetrabutylammoniumperchlorate (TBAP) (0.10 M) was added as the supporting electrolyte. Electrochemical spectra were measured at the potentials applied in the range from 0 to −1.3 volt.

The cyclic voltammograms of the synthesized uranyl complexes all exhibit a quasi-reversible redox process which is most likely due to the $\{UO_2\}^{2+}/\{UO_2\}^{+}$ couple.

The electron density on U^V atom is larger than that on U^{VI} atom because unlike $U^{VI}O_2^{2+}$, $U^VO_2^+$ has one 4f electron. Upon reversal of the scan direction, the U(V) complex is oxidized to U(VI) at overpotentials. The main influence on the potential for the U(VI)/U(V) couple of uranyl complexes is the level of π-donation from the ligand environment [35]. A typical cyclic voltammogram of $[UO_2(4\text{-Cl-saloph})(CH_3CN)]$ is shown in Fig. 5. The formal potentials ($E_{1/2}$(VI↔V)) for the U(V/VI) redox couple were calculated as the average of the cathodic (E_{pc}) and anodic (E_{pa}) peak potentials. The redox and formal potentials for the different complexes are collected in Table 5.

Biological activities of uranyl Schiff base complexes

This experiment is carried out on three complexes *D*, *E*, *F* and the results are well shown in the Fig. 6 and Table 6. By considering the results, it can be found that all the complexes have a good anticancer activity.

Table 4 The activation parameters of kinetics of TG studies

Compound	Slope	Intercept	T_S	E_a	A	ΔS	ΔH	ΔG
$[UO_2$(saloph)(MeOH)] 180°–230°	−3.45	0.37	216.9	66.1	2.5E7	−107.3	62.0	23.3
$[UO_2$(saloph)(MeOH)] 380°–420°	−4.99	0.88	400.9	95.5	1.19E8	−97.1	89.9	39.0
$[UO_2$(saloph)(MeOH)] 530°–545°	−2.82	2.73	537.5	53.9	1.9E4	−171.1	47.2	92.0
$[UO_2$(4-Me-saloph)(MeOH)] 175°–205°	−6.36	6.73	189.6	121.7	1.0E14	19.6	117.9	−3.6
$[UO_2$(4-Me-saloph)(MeOH)] 410°–450°	−2.57	2.99	443.3	49.2	9.5E3	−176.0	43.3	78.0
$[UO_2$(4-NO_2-saloph)(MeOH)] 28.5°–100°	−1.79	2.01	48.9	34.2	5.7E4	−155.1	31.3	11.6
$[UO_2$(4-NO_2 saloph)(MeOH)] 100°–190°	−0.50	5.54	184.5	9.7	14.4	−226.3	5.8	41.7
$[UO_2$(4-NO_2-saloph (MeOH)] 360°–410°	−1.13	4.90	408.0	21.7	79.3	−215.4	16.0	87.9
$[UO_2$(4-NO_2-saloph (MeOH)] 680°–705°	−1.80	4.38	690.3	34.5	389.1	−205.1	26.5	141.6
$[UO_2$(4-Cl-saloph)(MeOH)] 73–138 °C	−2.27	0.74	134.9	43.6	1.3E6	−130.3	40.2	17.6
$[UO_2$(4-Cl-saloph)(MeOH)] 388°–430°	−3.76	0.87	402.5	72.0	1.6E6	−132.6	66.4	53.4

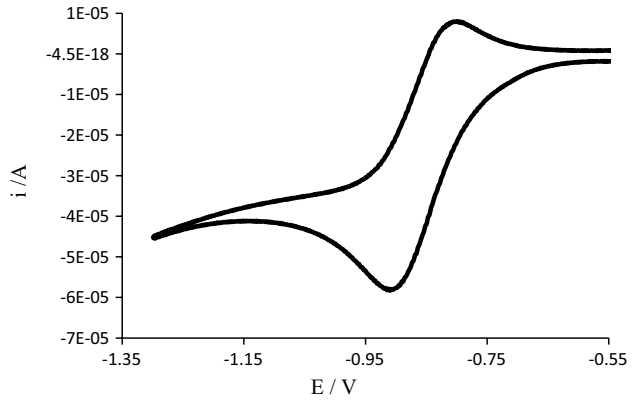

Fig. 5 The cyclic voltammogram of $[UO_2$(4-Cl-saloph)$(CH_3CN)]$

Table 5 The cyclic voltammetry data for uranyl compounds

Compounds	E_{ox}	E_{red}	ΔE
$[UO_2$(4-NO_2-saloph)$(CH_3CN)]$	−0.792	−0.93	−0.085
$[UO_2$(4-Cl-saloph)$(CH_3CN)]$	−0.799	−0.91	−0.083
$[UO_2$(saloph)$(CH_3CN)]$	−0.794	−0.91	−0.088
$[UO_2$(4-Me-saloph)$(CH_3CN)]$	−0.779	−0.93	−0.123

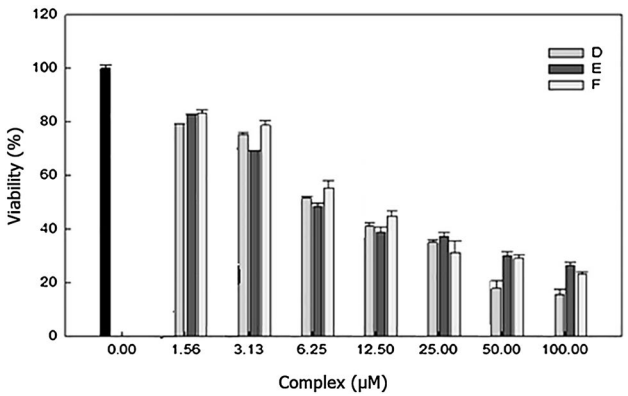

Fig. 6 Growth inhibition of the compounds investigated on Jurkat cell line for 24 h. Cell viability was evaluated by the MTT colorimetric assay. The *vertical bars* represent standard deviation of the triplicate determinations. *D* $[UO_2$(4-Cl-saloph)(DMSO)], *E* $[UO_2$(saloph)(DMSO)] and *F* $[UO_2$(4-Me-saloph)(DMSO)]

Table 6 The IC_{50} values (μm) of the ligands against Jurkat cell line

Ligand	*D*	*E*	*F*
IC50	7	6.15	9.6

Kinetic studies

When PBu_3 was added to the solution of the complex as a nucleophile, it occupied the sixth position in the equatorial plane in a rate-determining step, and then the solvent molecule was removed in a fast step.

The complete reaction was:

$$[UO_2(\text{Schiff base})(CH_3CN)] + PBu_3 \rightarrow [UO_2(\text{Schiff base})(PBu_3)] + CH_3CN$$

The pseudo-first-order constants were calculated by fitting data to Eq. 5:

$$\ln\left[(A_t - A_\infty)/(A_0 - A_\infty)\right] = -k_{obs}t \quad (5)$$

where A_t is the absorbance at time t; A_0 is the absorbance at $t = 0$; A_∞ is the absorbance at $t = \infty$. The parameter k_{obs} can be calculated from the slope of the linear plot of this equation versus time (t). As an example, the variation of the electronic spectra for $[UO_2(4\text{-Cl-saloph})(CH_3CN)]$, in the presence of PBu_3 (3 M), at 25 °C in acetonitrile is shown in Fig. 7.

PBu_3 with the excess concentration at least 1:10 was added to the uranyl complex solution. Therefore, the kinetics was followed under pseudo-first-order conditions. The rate law thus follows Eqs. (6, 7):

$$R = k_{obs}[\text{complex}] \quad (6)$$

$$k_{obs} = k_2[PBu_3] + k_1 \quad (7)$$

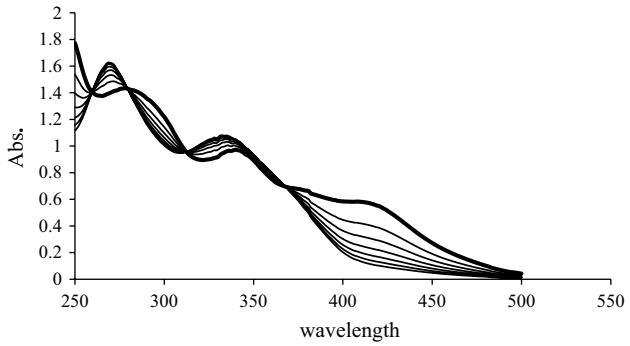

Fig. 7 The variation of electronic spectra of $[UO_2$ (4-Cl-saloph) $(CH_3CN)]$ with (PBu_3) in 20 °C

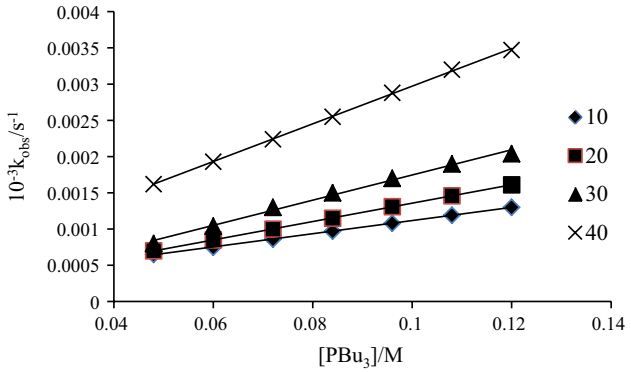

Fig. 8 Plots of k_{obs} versus PBu_3 for $[UO_2(4\text{-Cl-saloph})(CH_3CN)]$ complex at different temperatures 10–40 °C

where k_1 is the first-order rate constant for a solvent path; k_2 is the second-order rate constant. The second-order rate constants k_2 were obtained from the slope of the linear plots of k_{obs} versus $[PBu_3]$ (Fig. 8). By comparing k_2 in different temperatures, it could be concluded that the values of k_2 increased in high temperatures and the reaction rates increased too. The k_{obs} and k_2 values for all the complexes are collected in Tables 7, 8, 9 and 10. Activation parameters $\Delta H^{\#}$. and $\Delta S^{\#}$ were computed using k_2 values and Eyring equation (8);

$$\ln\left(\frac{k_2}{T}\right) = -\frac{\Delta H^{\#}}{RT} + \frac{\Delta S^{\#}}{R} + 23.8. \quad (8)$$

The plots of $\ln(k/T)$ versus $1/T$ provided $\Delta H^{\#}$ values from the slope of this chart and $\Delta S^{\#}$ from its intercept. The Eyring plot for the reaction of $[UO_2(4\text{-Cl-saloph})(CH_3CN)]$ with PBu_3 is shown in Fig. 9.

By using Eq. (9) $\Delta G^{\#}$ values could be obtained.

$$\Delta G^{\#} = \Delta H^{\#} - T\Delta S^{\#} \quad (9)$$

Table 11 shows the activation parameters $\Delta G^{\#}$ (at 40.0 °C), $\Delta H^{\#}$ and $\Delta S^{\#}$ for the reaction of the uranyl complexes with PBu_3 in CH_3CN. The large negative values for $\Delta S^{\#}$ and small values for $\Delta H^{\#}$ indicated an associative mechanism. The rate constants for the complexes due to their substitutional groups were as follows:

$$4 - NO_2 > 4 - Cl > H > 4 - Me$$

Table 7 Rate constants (k_2) and 10^3 k_{obs} for $[UO_2(\text{saloph})(CH_3CN)$ at different temperatures

10^2 [P]/M	10.8	12	13.2	14.4	15.6	16.8	18	10^2 k_2/M^{-1} s^{-1}
10 °C	1.18(0.11)	1.22(0.10)	1.28(0.44)	1.43(0.28)	1.53(0.32)	1.62(0.34)	1.73(0.34)	0.80(0.05)
20 °C	1.30(0.22)	1.41(0.10)	1.57(0.18)	1.74(0.14)	1.82(0.12)	1.91(0.26)	2.05(0.32)	1.04(0.05)
30 °C	1.48(0.31)	1.68(0.64)	1.82(0.28)	1.97(0.22)	2.16(0.12)	2.35(0.56)	2.47(0.62)	1.38(0.03)
40 °C	2.22(0.09)	2.36(0.07)	2.59(0.02)	2.90(0.02)	3.14(0.24)	3.42(0.14)	3.67(0.22)	2.00(0.07)

Numbers in parentheses are standard deviations

Table 8 Rate constants (k_2) and 10^3 k_{obs} for [UO_2(4-Me-saloph)(CH_3CN) at different temperatures

10^2 [P]/M	12	13.2	14.4	15.6	16.8	18.0	19.2	10^2 k_2/M^{-1} s^{-1}
10 °C	1.10(0.08)	1.21(0.06)	1.32(0.08)	1.35(0.10)	1.41(0.14)	1.50(0.10)	1.58(0.24)	0.63(0.04)
20 °C	1.33(0.09)	1.43(0.03)	1.55(0.02)	1.67(0.02)	1.75(0.03)	1.81(0.05)	2.02(0.14)	0.90(0.05)
30 °C	1.59(0.21)	1.71(0.24)	1.86(0.10)	2.00(0.14)	2.14(0.06)	2.28(0.04)	2.43(0.03)	1.17(0.01)
40 °C	1.87(0.41)	2.21(0.44)	2.26(0.47)	2.45(0.30)	2.64(0.30)	2.70(0.30)	3.01(0.14)	1.42(0.11)

Numbers in parentheses are standard deviations

Table 9 Rate constants (k_2) and 10^3 k_{obs} for [UO_2(4-Nitro-saloph)(CH_3CN) at different temperatures

10^2 [P]/M	1.2	2.4	3.6	4.8	6.0	7.2	8.4	10^2 k_2/M^{-1} s^{-1}
10 °C	0.42(0.32)	0.70(0.21)	0.91(0.12)	1.14(0.10)	1.39(0.05)	1.67(0.07)	1.95(0.11)	2.00(0.04)
20 °C	0.52(0.14)	0.88(0.11)	1.14(0.04)	1.38(0.02)	1.79(0.09)	2.16(0.21)	2.48(0.34)	2.70(0.08)
30 °C	0.68(0.44)	1.18(0.31)	1.69(0.20)	2.19(0.08)	2.71(0.05)	3.21(0.10)	3.71(0.37)	4.22(0.00)
40 °C	1.22(0.40)	2.04(0.33)	2.80(0.34)	3.57(0.23)	4.05(0.12)	4.90(0.08)	5.71(0.38)	6.00(0.14)

Numbers in parentheses are standard deviations

Table 10 Rate constants (k_2) and 10^3 k_{obs} for [UO_2(4-Cl-saloph)(CH_3CN) at different temperatures

10^2 [P]/M	4.8	6.0	7.2	8.4	9.6	1.08	1.2	10^2 k_2/M^{-1} s^{-1}
10 °C	0.65(0.10)	0.75(0.10)	0.86(0.10)	0.97(0.10)	1.08(0.10)	1.19(0.20)	1.30(0.20)	9.00(0.00)
20 °C	0.70(0.10)	0.85(0.10)	1.00(0.02)	1.15(0.08)	1.31(0.10)	1.46(0.10)	1.61(0.20)	1.27(0.00)
30 °C	0.80(0.04)	1.04(0.03)	1.30(0.03)	1.50(0.20)	1.70(0.20)	1.90(0.06)	2.04(0.20)	1.74(0.06)
40 °C	1.62(0.07)	1.93(0.2)	2.24(0.10)	2.55(0.06)	2.88(0.09)	3.20(0.09)	3.47(0.05)	2.50(0.02)

Numbers in parentheses are standard deviations

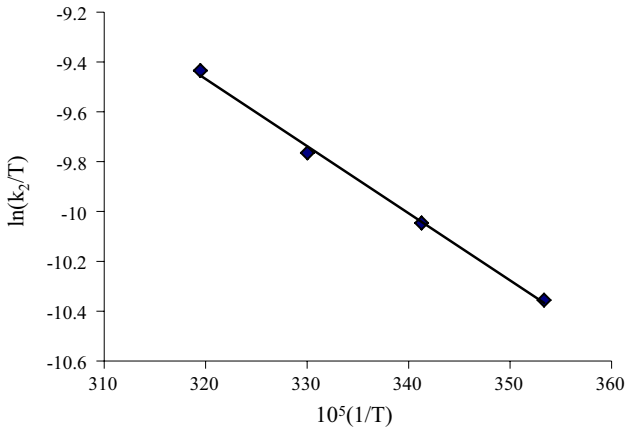

Fig. 9 Plot of ln(k_2/T) versus (1/T) for [UO_2(4-Cl-saloph)(CH_3CN)] complex

Electronic factor was important. The electron-withdrawing groups such as Cl, NO_2 made the uranium center more positive; therefore, the rate of the substitution reaction increased. The electron-releasing group such as Me decreased it [36].

The effect of solvent on the kinetic of substitution reaction

The stability and equilibrium constant between two complexes with different coordination numbers are usually related to solvent. For studying the effect of solvent on the rate constant (k_2) of pentavalent-uranyl Schiff base complexes, the interaction of the complexes with tributylphosphine in THF and acetonitrile was carried out. The variation of electronic spectrum of [UO_2(saloph)(THF)] with PBu_3 is shown in Fig. 10. The k_{obs} and k_2 values for [UO_2(saloph)(THF)] complex with PBu_3 are collected in Table 12. The rate constants (10^2 k_2) and the activation parameters for reaction of [UO_2(saloph)] with (PBu_3) were compared for two solvents and collected in Tables 13 and 14.

These results showed that the rate constants depended on the solvent and the trend was related to the donor number of the solvent. The Gutmann donor number for CH_3CN

Table 11 The values of activation parameters for uranyl complexes

Complex	$10^5\ \Delta H^{\#}$/kJmol^{-1}	$\Delta S^{\#}$/JK^{-1}mol^{-1}	$\Delta G^{\#a}$/kJmol^{-1}
[UO_2(4-NO_2-saloph)(CH_3CN)]	25.3(1.7)	−189.1(5. 8)	55.4(1.8)
[UO_2(4-Cl-saloph)(CH_3CN)]	22.4(0.8)	−204.9(2.7)	60.0(0.9)
[UO_2(saloph)(CH_3CN)]	19.8(1.7)	−215.3(5.8)	63.1(1.8)
[UO_2(4-Me-saloph)(CH_3CN)]	17.5(1.5)	−224.9(5.1)	65.1(1.6)
[UO_2(saloph)(THF)]	17.8(0.3)	−223.0(0.9)	65.3(0.3)

Numbers in parentheses are standard deviations

[a] $\Delta G^{\#}$ was calculated at $T = 20$ °C

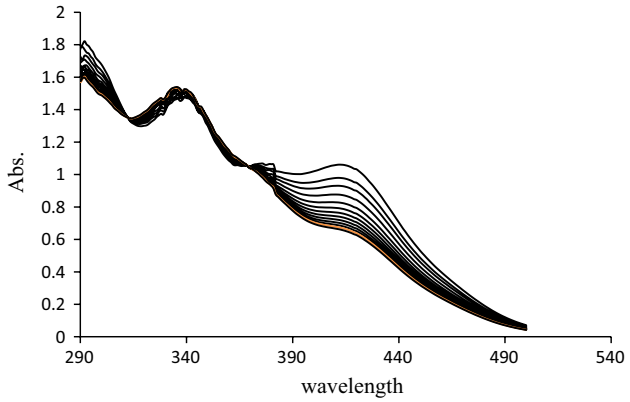

Fig. 10 The variation of electronic spectra of [UO_2(saloph)(THF)] with PBu_3

is 14.1 and for THF it is 20. The rate constants in THF with higher donor number were smaller than the rate constants in CH_3CN because the five-coordinated complex was more stable in a solvent with higher donor number. In other words, a solvent with higher donor number better coordinated to a five-coordinated complex and stabilized it. Therefore the trend of the reactivity of the studied complexes and rate constants toward PBu_3 according to the solvent was as follows: CH_3CN > THF.

Conclusion

Several tetradentate uranyl Schiff base complexes were synthesized and characterized by different techniques. For one of them which was also prepared in nano form, TEM images showed nano-particles with sizes between 30 and 35 nm. X-ray structure of [UO_2(4-NO_2-saloph)(DMF)] confirmed that the solvent molecule occupied the fifth position of the equatorial plane of the distorted pentagonal–bipyramidal structure. The presence of one coordinated solvent molecule was also confirmed by thermal gravimetric studies. The kinetic of complex decomposition was studied by using thermogravimetric method (TG). For all the complexes, the Gibbs free energy (ΔG) grew from stage to stage. This was probably due to the stable intermediate of the present stages. According to coats-Redfern plots, the kinetic of thermal decomposition of studied complexes was first-order in all stages.

Table 12 Rate constants (k_2) and $10^3\ k_{obs}$ for [UO_2(saloph)(THF)] at different temperatures

10^2 [P]/M	12.0	13.2	14.4	15.6	16.8	18.0	19.2	$10^2\ k_2$/M^{-1} s^{-1}
10 °C	1.70(0.10)	1.73(0.20)	1.82(0.10)	1.91(0.10)	2.02(0.08)	2.11(0.06)	2.17(0.1)	0.70(0.03)
20 °C	1.86(0.20)	2.00(0.20)	2.13(0.20)	2.25(0.20)	2.37(0.10)	2.45(0.10)	2.55(0.03)	0.95(0.03)
30 °C	2.25(0.20)	2.50(0.20)	2.65(0.10)	2.78(0.10)	2.92(0.10)	3.06(0.10)	3.19(0.07)	1.25(0.06)
40 °C	2.90(0.20)	3.10(0.04)	3.35(0.04)	3.56(0.07)	3.70(0.07)	3.88(0.09)	4.06(0.2)	1.60(0.05)

Numbers in parentheses are standard deviations

Table 13 The rate constant ($10^2\ k_2$), for [UO_2(saloph)] with (PBu_3)

Solvent	Donor number	$10^2\ K_2$			
		10 °C	20 °C	30 °C	40 °C
Acetonitril	14.1	0.80(0.05)	1.04(0.05)	1.38(0.03)	2.00(0.07)
THF	20	0.70(0.03)	0.95(0.03)	1.25(0.06)	1.60(0.05)

Numbers in parentheses are standard deviations

Table 14 The activation parameters $\Delta H^{\#}$, $\Delta S^{\#}$, $\Delta G^{\#}$, for $[UO_2(saloph)]$ with PBu_3

Solvent	$10^5\ \Delta H^{\#}/kJmol^{-1}$	$\Delta S^{\#}/JK^{-1}mol^{-1}$	$\Delta G^{\#}/kJmol^{-1}$
CH_3CN	19.8(1.8)	−215.3(5.9)	63.1(1.8)
THF	17.8(0.3)	−223.0(0.9)	65.3(0.3)

Numbers in parentheses are standard deviations

Cyclic voltammetry of the uranyl complexes showed that in acetonitrile solution uranium had two oxidation states [U(VI) ↔ (V)]. All the complexes had good anticancer activity. In kinetic studies, low values of $\Delta H^{\#}$, and the large negative $\Delta S^{\#}$ values revealed that the mechanism of the substitution reaction was an associative one. The rate constants for the complexes, due to their substitutional groups, proved that an acceptor group increased the reaction rate while a donor group decreased it. Thus the following trends were observed: 4-NO_2 > 4-Cl > H > 4-Me. The rate constants depended on the solvent, therefore in THF solvent with higher donor number the rate constants were smaller than in CH_3CN. The following trends were observed for k_2 and rate constants values: $[UO_2(saloph)(CH_3CN)] > [UO_2(saloph)(THF)]$.

Acknowledgments We are grateful to Shiraz University Research Council for its financial support. The crystallographic part was supported by the project 14-03276S of the Czech Science Foundation.

Appendix 1: Supplementary material

CCDC 914883 contains the supplementary crystallographic data for this paper. These data can be obtained free of charge from The Cambridge Crystallographic Data Centre via www.ccdc.cam.ac.uk/data_request/cif.

References

1. V.P. Lozitsky, V.E. Kuzmin, A.G. Artemenko, R.N. Lozitska, A.S. Fedtchouk, E.N. Muratov, A.K. Mescheriakov, SAR QSAR Environ. Res. **16**, 219 (2005)
2. D. Sinha, A.K. Tiwari, S. Singh, G. Shukla, P. Mishra, H. Chandra, A.K. Mishra, Eur. J. Med. Chem. **43**, 160 (2008)
3. S. Adsule, V. Barve, D. Chen, F. Ahmed, Q.P. Dou, S. Padhye, F.H. Sarkar, J. Med. Chem. **49**, 7242 (2006)
4. S. Ren, R. Wang, K. Komatsu, P. Bonaz-Krause, Y. Zyrianov, C.E. McKenna, C. Csipke, Z.A. Tokes, E.J. Lien, J. Med. Chem. **45**, 410 (2002)
5. Z.H. Abd El-Wahab, M.R. El-Sarrag, Spectrochim. Acta Part A **60**, 271 (2004)
6. E. Yoshida, S. Yamada, Bull. Chem. Soc. Jpn. **40**, 1395 (1967)
7. A. Elmali, C.T. Zeyrek, Y. Elerman, T.N. Durlu, J. Chem. Crystallogr. **30**, 167 (2000)
8. A.A. Soliman, W. Linert, Thermochim. Acta **338**, 67 (1999)
9. S. Zolezzi, A. Decinti, E. Spodine, Polyhedron **18**, 897 (1999)
10. G. Gordon, H. Taube, J. Inorg. Nucl. Chem. **16**, 272 (1961)
11. W. Jung, Y. Ikeda, H. Tomiyasu, H. Fukutomi, Bull. Chem. Soc. Jpn. **57**, 2317 (1984)
12. Y. Kato, H. Fukutomi, J. Inorg. Nucl. Chem. **38**, 1323 (1976)
13. K. Okuyama, Y. Ishikawa, Y. Kato, H. Fukutomi, Bull. Res. Lab. Nucl. React. **3**, 39 (1978)
14. S.F. Lincoln, Pure Appl. Chem. **51**, 2059 (1979)
15. H. Tomiyasu, H. Fukutomi, Bull. Res. Lab. Nucl. React. **7**, 57 (1982)
16. E. Comini, Anal. Chim. Acta **568**, 28 (2006)
17. N. Kocak, M. Sahin, S. Kucukkolbasi, Z.O. Erdogan, Int. J. Biol. Macromol. **51**, 1159 (2012)
18. H.L. Karlsson, J. Gustafsson, P. Cronholm, L. Moller, Toxicol. Lett. **188**, 112 (2009)
19. L. Palatinus, G. Chapuis, J. Appl. Cryst. **40**, 786 (2007)
20. V. Petricek, M. Dusek, L. Palatinus, Z. Kristallogr. **229**, 345 (2014)
21. T. Mossman, J. Immunol. Methods **65**, 55 (1983)
22. D.J. Evans, P.C. Junk, M.K. Smith, Polyhedron **21**, 2421 (2002)
23. K. Mizuoka, Y. Ikeda, Inorg. Chem. **42**, 3396 (2003)
24. S.Y. Ebrahimipour, J.T. Mague, A. Akbari, R. Takjoo, J. Mol. Struct. **1028**, 148 (2012)
25. M. Ebel, D. Rehder, Inorg. Chem. **45**, 7083 (2006)
26. D.N. Kumar, B.S. Garg, Spectrochim. Acta, Part A **64**, 141 (2006)
27. U. Casellato, S. Tamburini, P. Tomasin, P.A. Vigato, Inorg. Chim. Acta **341**, 118 (2002)
28. M.S. Bharara, K. Heflin, S. Tonks, K.L. Strawbridge, A. E. V. Gorden. Dalton Trans. **10**, 2966 (2008)
29. A.H. Kianfar, M. Dostani, Spectrochim. Acta, Part A **82**, 69 (2011)
30. Z. Asadi, F. Golzard, V. Eigner, M. Dusek, J. Coord. Chem. **66**, 3629 (2013)
31. M.S. Refat, M.Y. El-Sayed, A.M.A. Adam, J. Mol. Struct. **1038**, 62 (2013)
32. Z. Asadi, M.R. Shorkaei, Spectrochim. Acta, Part A **105**, 344 (2013)
33. A.W. Coats, J.P. Redfern, Nature **201**, 68 (1964)
34. Z. Asadi, M. Asadi, F.D. Firuzabadi, R. Yousefi, M. Jamshidi, J. Iran. Chem. Soc. **11**, 423 (2014)
35. H.C. Hardwick, D.S. Royal, M. Helliwell, S.J.A. Pope, L. Ashton, R. Goodacred, C.A. Sharrad, Dalton Trans. **40**, 5939 (2011)
36. Z. Asadi, M. Asadi, F.D. Firuzabadi, Int. J. Chem. Kinet. **45**, 795 (2013)